Japanese Journal of Applied Physics

REGULAR PAPERS

Ultrafast microscopy in resolving femtosecond laser-induced surface structuring

Japanese Journal of Applied Physics **57**, 08PF04 (2018)
https://doi.org/10.7567/JJAP.57.08PF04

REGULAR PAPER

Ultrafast microscopy in resolving femtosecond laser-induced surface structuring

Ranran Fang[1,2], Anatoliy Y. Vorobyev[1], Subhash C. Singh[1,3], and Chunlei Guo[1,3*]

[1]*The Institute of Optics, University of Rochester, Rochester, NY 14627, U.S.A.*
[2]*School of Science, Chongqing University of Posts and Telecommunications, Chongqing 400065, China*
[3]*Changchun Institute of Optics, Fine Mechanics, and Physics, Changchun 130033, China*

*E-mail: guo@optics.rochester.edu

Received January 10, 2018; revised April 29, 2018; accepted April 30, 2018; published online July 18, 2018

In this work, using a high-contrast scattered-light-based optical imaging technique, we capture the complete evolution of the femtosecond laser-induced surface structures of metals from the initial transient morphological fluctuation to the end of resolidification. We find that the initial transient surface structures appear at a delay time on the order of 100 ps following laser irradiation. Both temporal and spatial evolution of the transient surface structures depend on laser fluence. The major mechanism of the transient surface structures is ablation driven by pressure relaxation in the surface layer. The ablation mechanism is identified as phase explosion by estimating the surface temperatures at the studied fluence. The temporal evolution of the solidification process is found to be significantly slower than previously predicted by theoretical models.

1. Introduction

Surface nano/microstructures play an important role in modifying physical, chemical, and biomedical properties of materials.[1–4] A number of studies have demonstrated that a femtosecond ablation technique for surface nano/microstructuring is capable of controllably producing a large variety of surface structures in terms of their morphology and dimensions,[5–8] while femtosecond spectroscopy can diagnose electron dynamics in atomic and molecular systems.[9] These studies have resulted in the creation of novel materials, including black silicon,[5] black metals,[10,11] colored metals,[12–14] superhydrophobic,[15–18] superhydrophilic/superwicking,[19] biomedical,[18,20–23] and multifunctional[24] materials. Although extensive works have been devoted to the formation mechanisms of laser-induced surface structures,[6,12,25–28] there still lacks a clear understanding of the involved physical processes. In this paper, to further understand the physical processes governing the formation of the femtosecond laser-induced surface structures on metals, we perform a time-resolved study of surface morphology following ultrafast laser pulse excitation. The evolution of the surface morphology is studied using a high-contrast scattered-light-based optical imaging technique. In contrast to the conventional femtosecond laser pump–probe microscopy based on specular reflections,[29–34] the scattered-light imaging provides a near-zero background and high contrast, allowing us to obtain clear images of the surface morphological changes. Our study is focused on laser-induced nano/microstructures, which are commonly generated at low and moderate laser fluence.[6] Using our time-resolved imaging technique, we find three characteristic times in the evolution of laser-induced surface nano/microstructures: the time when structures start to form on the melted surface, the time when the solidification of the surface structures begins, and the time when the surface structures become completely solidified.

2. Experimental methods

The configuration of our experimental setup is reported previously[35] and is shown in Fig. 1. An amplified Ti:sapphire laser system generating 65-fs pulses with pulse energy up to 1 mJ at a 1-kHz repetition rate with the central wavelength at 800 nm is used in our experiment. Using an electromechanical shutter, we select a single pulse from a pulse train generated by the laser system. A beam splitter is used to form pump and probe beams. A pump beam produces surface structures on a studied sample through ablation. The incidence angle of the pump beam is 36°. The studied metal is polished bulk zinc (Zn). The probe beam is used for stroboscopic illumination of the spot ablated by the pump pulse. An optical delay line provides various delay times between the pump and probe pulses in the range between 0 fs and 408 ns. The delay line shown schematically in Fig. 1 relates to the longest delay time of 408 ns, and its total length is about 122 m. For the delay times between 408 and 1 ns, a sequence of flip mirrors were used. However, for delays less than 1 ns, we used a flip mirror mounted on a computer controlled translation stage.

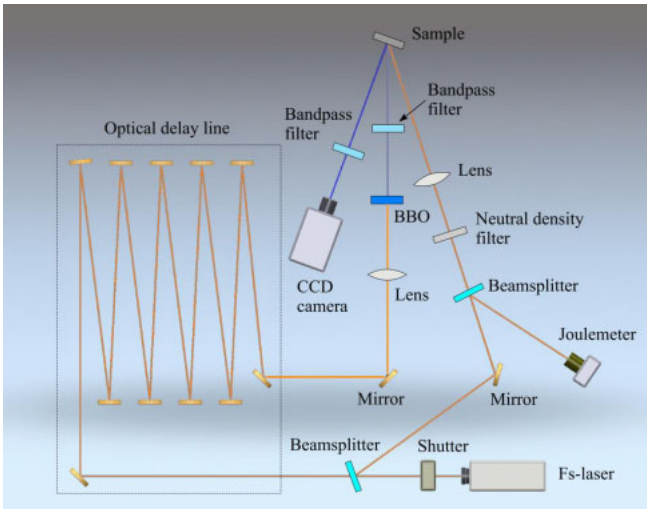

Fig. 1. (Color online) Ultrafast pump–probe imaging setup.

Using a BBO crystal, the main pulse at 800 nm is converted to second harmonic at 400 nm. A blue band-pass filter blocks fundamental radiation passed through the BBO crystal. The 400-nm probe pulse is directed onto the sample at an incidence angle of 18°. The incident angles for pump and probe beams have been optimized from our test experiments in obtaining the best image quality of the surface

structures. A long-working distance objective is used for imaging the sample surface onto a sensor of a CCD camera. The CCD camera is aligned normal to the sample surface. A 400-nm band-pass filter placed in front of the imaging objective blocks scattered pump radiation. The imaging optics we use is capable of resolving both microscale clusters of nanostructures and microstructures. For each fixed delay time, we capture a sequence of three surface images. The first surface image is taken at 10 s before the pump laser pulse irradiation for identifying initial structures present on the surface, if any. The second image of the surface is captured at a preset time delay. The third surface image is taken at 10 s after the pump laser pulse irradiation to record the final surface structure produced by the laser pulse. Taking this sequence of the surface images at various delay times allows us to track the formation of the surface structures in time. In this work, the evolution of surface nano/microstructures is studied at laser fluence $F = 0.14$ and $0.78\,\mathrm{J/cm^2}$. A scanning electron microscope (SEM) is used to examine the laser-induced surface nano/microstructures after resolidification of the surface.

3. Results and discussion

The CCD images of zinc surface captured at different delay times after a pump laser pulse with laser fluence of 0.14 $\mathrm{J/cm^2}$ are shown in Fig. 2. One can see that the surface structural changes begin to occur at a time of about $t = 300$ ps [Fig. 2(c)]. A comparison of these surface structures with those taken at a long time after laser pulse ($t = \infty$) [Fig. 2(d)] shows that they are completely different, indicating that the material in the irradiated spot is not yet solidified and the observed surface structure is transient. At laser fluence of $0.14\,\mathrm{J/cm^2}$, the characteristic time of the surface melting following irradiation of Zn with femtosecond laser pulse is about 3 ps.[34] Therefore, our experiment shows that the irradiated surface does not undergo morphological modifications immediately after melting, and there is a delay time between melting and hydrodynamic motion of the melted material resulting in the transient morphological changes on the surface. The comparison of Figs. 2(e) and 2(f) demonstrates that the solidification of surface structures begins at $t = 860$ ps and this process first occurs on the periphery of the irradiated spot. With further increasing the delay time, the solidified area increases. Figures 2(g) and 2(h) show that about 60% of the surface structures are solidified at $t =$ 124 ns. Finally, Figs. 2(i) and 2(j) show that the surface structure becomes completely solidified at $t = 322$ ns. Thus, from this imaging data we find three important characteristic times in the dynamics of surface structures: the time when the surface structures begin to appear (300 ps), the time when the surface structures begin to solidify (860 ps), and the time when the surface structure becomes completely solidified (322 ns). SEM images of surface nano/microstructures produced in the center of the ablated spot at the studied laser fluence of $0.14\,\mathrm{J/cm^2}$ are shown in Fig. 3, where both nanostructures with the size in a range of 30–500 nm and fine microstructures are seen.

Snapshots of the transient surface structures at different delay times at laser fluence of $0.78\,\mathrm{J/cm^2}$ are shown in Fig. 4. It is seen in Fig. 4(a) that the surface structures first appear on the edge of the irradiated spot and form a ring, in contrast to ablation at $F = 0.14\,\mathrm{J/cm^2}$, where the surface structures first appear in the center of the irradiated spot [Fig. 2(c)]. With time, the transient surface structures move towards the center of the irradiated spot and populate its central part. The whole

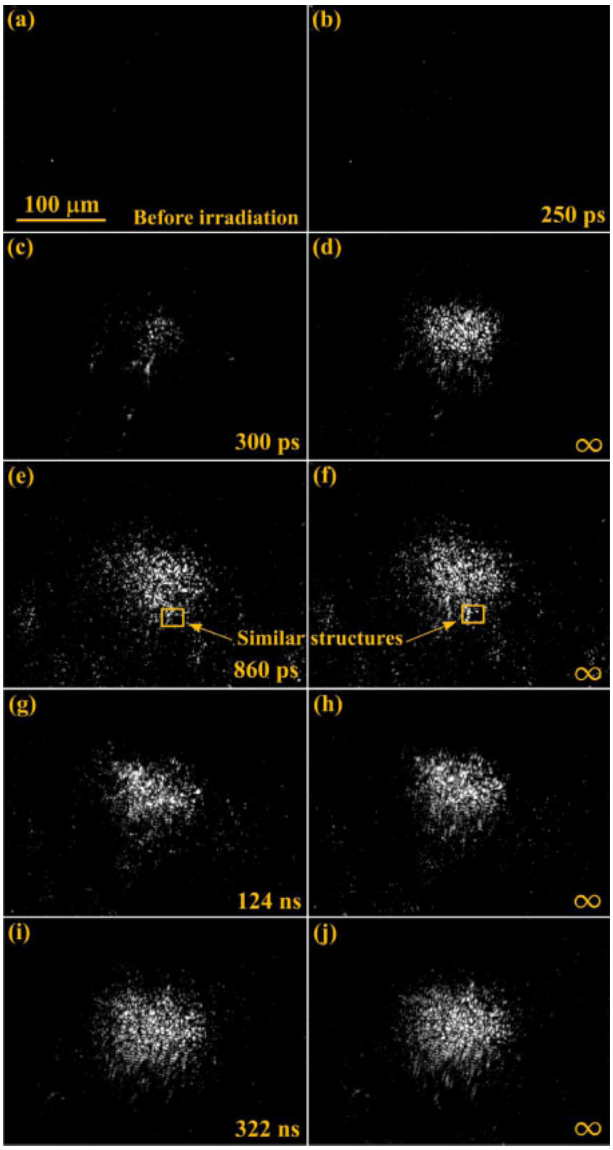

Fig. 2. (Color online) A comparison of transient surface structures at various delay times and final solidified structures following the pump laser pulse at laser fluence of $0.14\,\mathrm{J/cm^2}$.

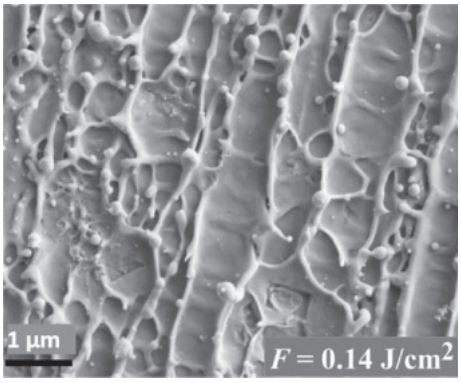

Fig. 3. SEM images of surface nano/microstructures on Zn surface produced in the center of the ablated spot with $F = 0.14\,\mathrm{J/cm^2}$ of laser fluence.

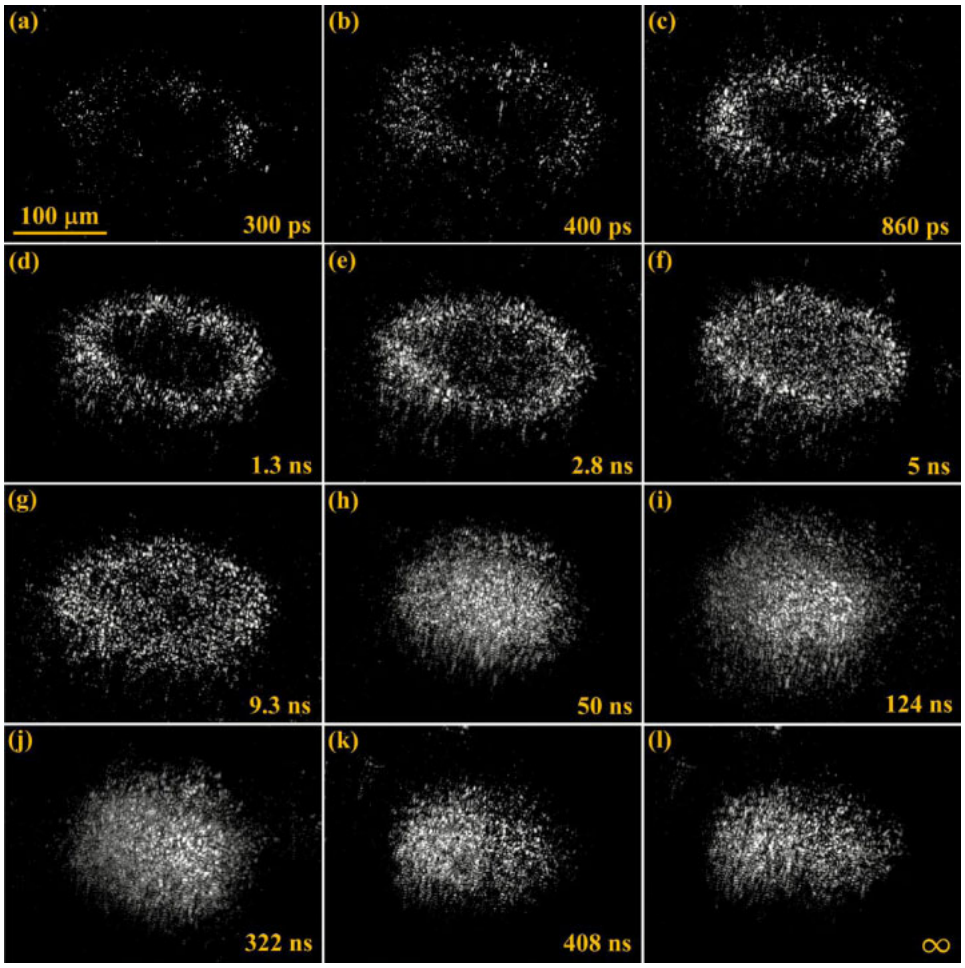

Fig. 4. (Color online) Images of zinc surface at various delay times following a pump laser pulse at $F = 0.78\,\mathrm{J/cm^2}$.

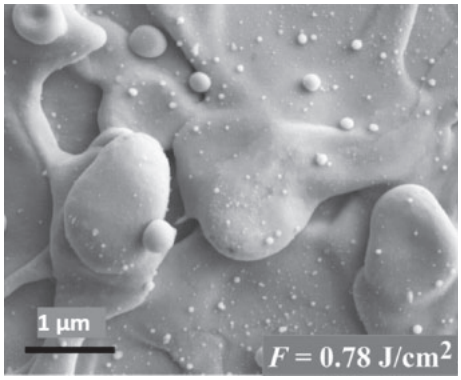

Fig. 5. SEM images of surface nano/microstructures on Zn surface produced in the center of the ablated spot with $F = 0.78\,\mathrm{J/cm^2}$ of laser fluence.

ablation area becomes covered with structures at about 5 ns [Fig. 4(f)]. The solidification of the transient surface structures begins at about 50 ns. At the longest time delay available in our experiments (408 ns), the solidification of surface structures is not completed as seen from the comparison of Figs. 4(k) and 4(l). The SEM image of the surface ablated at $F = 0.78\,\mathrm{J/cm^2}$ shown in Fig. 5 demonstrates that the microscale surface structures are the major morphological feature at this laser fluence. The nanostructures seen in Fig. 5 mostly originate from redeposition of ablated nanoparticles.

The formation of the transient and permanent (solidified) surface structures is driven by several mechanisms, including pressure relaxation in molten surface layer, ablation, Marangoni effect, and contraction of a material in solidification process. The mechanism of pressure relaxation in molten surface layer is governed by the speed of sound in the liquid material,[36,37] and can be estimated by $t_P \approx L/v_{sl}$, where v_{sl} is the speed of sound in liquid Zn and L is the typical radial size of the surface structures. This mechanism is fast and can induce transient surface nanostructural fluctuations on the picoseconds time scale even before ablation onset at low laser fluence near the ablation threshold.[38] The appearance of the surface structures first on the edge of the irradiated spot at $F = 0.78\,\mathrm{J/cm^2}$ (Fig. 4) can be explained by two possible mechanisms. First one may be related to the presence of mirror like surface from melted phase at the center due to the Gaussian distribution of laser intensity and hence no or comparatively smaller scattering signal. Higher fluence at the center will produce more volume of melting that would take longer time than peripheral region to get solidify. Another mechanism may be related to the plasma screening. When the pressure in the surface layer is high, its relaxation results in ablation, and the formation of the transient surface structures will be inherently associated with the processes of material removal from the surface and recoil pressure of the ablated material.[39] The Marangoni effect is the flow of the melted material due to the temperature gradient and typically occurs on the nanosecond

time scale.[40,41] Among all described above mechanism, ablation has a major impact on the transient surface structures and the identification of the ablation mechanism at the studied here laser fluences is critically important.

There are several ablation mechanisms of metals,[42–44] including evaporation,[45] thermomechanical fragmentation/spallation,[46–51] and phase explosion.[46,48,52–54] To identify the ablation mechanisms in our experiments, we estimate the maximum lattice temperature T_{im} using the formula,[34,55]

$$T_{im} \approx T_0 + \frac{F_A}{c_i}\frac{\beta\alpha}{\beta+\alpha}, \quad \beta = \sqrt{\frac{g}{k}}, \tag{1}$$

where T_0 is the room temperature, c_i is the specific heat of the lattice, α is the absorption coefficient, g is the electron–phonon coupling factor, k is the thermal conductivity, and $F_A = (1-R)F$ is the absorbed laser fluence, where R is the reflectance of Zn at the laser wavelength. The reflectance of real metallic surfaces depends on the sample structural defects remaining after polishing, contaminants, angle of incidence, and laser fluence.[56] Therefore, to obtain a reliable estimation of the surface temperature, we measure the reflectance of our sample under the same experimental conditions used in the surface imaging experiment. Using a hemi-ellipsoidal metallic reflector technique,[56] the reflectance of our zinc sample was measured to be 0.57 and 0.56 at laser fluence of 0.14 and 0.78 J/cm^2, respectively. The values of the maximum surface temperature estimated using $T_0 = 300$ K, $c_i = 2.78 \times 10^6$ J m^{-3} K^{-1},[55] $\alpha = 7.5 \times 10^7$ m^{-1},[57] $g = 6 \times 10^{16}$ W m^{-3} K^{-1},[57] and $k = 116$ W m^{-1} K^{-1} are 4079 and 21840 K at $F = 0.14$ and 0.78 J/cm^2, respectively. These values of the surface temperature exceed the thermodynamic critical point T_c of zinc (3190 K), suggesting that the ablation mechanism at the studied laser fluence values is the phase explosion.[54] Therefore the observed transient surface structures caused by ablation are associated with the phase explosion mechanism. When ablation ends, the residual liquid surface layer cools and solidifies, resulting in permanent surface structures. Available in the literature theoretical models of cooling process based on the electron heat conduction mechanism predict the times of complete solidification to be 2.5 ns for Al[58] and 1.4–1.7 ns for Ag,[59] which are by two orders smaller the observed value in our study for Zn (322 ns). This disagreement indicates that cooling process following ablation is more complicated. We speculate that the cooling process can be slowed down by the effect of enhanced thermal coupling observed in works,[60–62] where it has been found that a significant amount of thermal energy remains in a metal following femtosecond laser ablation due to the transfer of thermal energy from ablation plume back to the sample on the timescale long after the laser pulse. Furthermore, the surface cooling can be also slowed down by the latent heat released in solidification process and exothermic chemical reactions induced in laser ablation.[62–64] For example, it has been previously found that the contribution of the chemical source of energy can reach up to 30% of incident laser energy in nanosecond laser ablation of Zn in air environment.[65]

4. Conclusion

In this work, we study the dynamics of surface nano/microstructures induced on the surface of zinc in femtosecond laser ablation using the scattered-light pump–probe optical microscopy. We find important characteristic times in the dynamics of laser-induced surface structures: the time when the surface structures begin to appear, the time when the surface structures begin to solidify, and the time when the surface structure becomes completely solidified. We find that the transient surface nano/microstructures appear at a delay time on the order of 100 ps following laser irradiation. The time of the transient surface structure onset is a function of laser fluence, namely, the higher laser fluence, the shorter the transient surface structure onset time. At low laser fluence favorable for producing nanostructures, the transient surface structures first appear in the central portion of the ablated spot. At high laser fluence favorable for producing microstructures in the central part of ablated spot, the transient surface structures first appear on the periphery of the ablated spot, where laser fluence is smaller and favorable for generating nanostructures. The observed solidification onset time is laser-fluence dependent, namely, the higher laser fluence, the longer solidification onset time. The observed time for complete solidification is significantly longer then theoretically predicted one. We speculate that this significant decrease of cooling rate is dominantly caused by the effect of enhanced thermal coupling.

Acknowledgments

This work was supported by Bill & Melinda Gates Foundation and US Army Research Office. This work was also supported by the National Natural Science Foundation of China No. 10904177 and Chongqing Municipal Education Commission No. KJ1400438.

1) K. M. T. Ahmmed, C. Grambow, and A. M. Kietzig, Micromachines **5**, 1219 (2014).
2) A. Y. Vorobyev and C. Guo, Laser Photonics Rev. **7**, 385 (2013).
3) L. Li, M. Hong, M. Schmidt, M. Zhong, A. Malshe, B. H. Veld, and V. Kovalenko, CIRP Ann.—Manuf. Technol. **60**, 735 (2011).
4) J. Cheng, C. S. Liu, S. Shang, D. Liu, W. Perrie, G. Dearden, and K. Watkins, Opt. Laser Technol. **46**, 88 (2013).
5) R. Younkin, J. E. Carey, E. Mazur, J. A. Levinson, and C. M. Friend, J. Appl. Phys. **93**, 2626 (2003).
6) A. Y. Vorobyev and C. Guo, Opt. Express **14**, 2164 (2006).
7) B. K. Nayak and M. C. Gupta, Opt. Lasers Eng. **48**, 940 (2010).
8) C. A. Zuhlke, T. P. Anderson, and D. R. Alexander, Opt. Express **21**, 8460 (2013).
9) G. Rodriguez, C. W. Siders, C. Guo, and A. J. Taylor, IEEE J. Sel. Top. Quantum Electron. **7**, 579 (2001).
10) A. Y. Vorobyev and C. Guo, Phys. Rev. B **72**, 195422 (2005).
11) A. Y. Vorobyev and C. Guo, Appl. Phys. Lett. **92**, 041914 (2008).
12) E. Stratakis, V. Zorba, M. Barberoglou, C. Fotakis, and G. Shafeev, Nanotechnology **20**, 105303 (2009).
13) B. Dusser, Z. Sagan, H. Soder, N. Faure, J. P. Colombier, M. Jourlin, and E. Audouard, Opt. Express **18**, 2913 (2010).
14) T. Baldacchini, J. E. Carey, M. Zhou, and E. Mazur, Langmuir **22**, 4917 (2006).
15) V. Zorba, L. Persano, D. Pisignano, A. Athanassiou, E. Stratakis, R. Cingolani, P. Tzanetakis, and C. Fotakis, Nanotechnology **17**, 3234 (2006).
16) A. M. Kietzig, S. G. Hatzikiriakos, and P. Englezos, Langmuir **25**, 4821 (2009).
17) E. Fadeeva, S. Schlie, J. Koch, B. N. Chichkov, A. Y. Vorobyev, and C. Guo, in *Contact Angle, Wettability and Adhesion*, ed. K. L. Mittal (VSP International Science, Leiden, 2009) Vol. 6, p. 163.
18) A. Y. Vorobyev and C. Guo, Appl. Phys. Lett. **94**, 224102 (2009).
19) A. Y. Vorobyev and C. Guo, Appl. Surf. Sci. **253**, 7272 (2007).
20) E. Stratakis, A. Ranella, and C. Fotakis, Biomicrofluidics **5**, 013411 (2011).
21) A. Y. Vorobyev and C. Guo, Appl. Phys. Lett. **99**, 193703 (2011).

22) A. A. Ionin, S. I. Kudryashov, S. V. Makarov, P. N. Saltuganov, L. V. Seleznev, D. V. Sinitsyn, E. V. Golosov, A. A. Goryainov, Y. R. Kolobov, K. A. Kornieieva, A. N. Skomorokhov, and A. E. Ligachev, Laser Phys. Lett. **10**, 045605 (2013).
23) A. Y. Vorobyev and C. Guo, J. Appl. Phys. **117**, 033103 (2015).
24) T. Y. Hwang, A. Y. Vorobyev, and C. Guo, Appl. Phys. Lett. **95**, 123111 (2009).
25) V. V. Zhakhovskii, N. A. Inogamov, and K. Nishihara, JETP Lett. **87**, 423 (2008).
26) B. J. Demaske, V. V. Zhakhovsky, N. A. Inogamov, and I. I. Oleynik, Phys. Rev. B **82**, 064113 (2010).
27) G. D. Tsibidis, E. Stratakis, and K. E. Aifantis, J. Appl. Phys. **111**, 053502 (2012).
28) M. C. Downer, R. L. Fork, and C. V. Shank, J. Opt. Soc. Am. B **2**, 595 (1985).
29) K. Sokolowski-Tinten, J. Bialkowski, A. Cavalleri, D. von der Linde, A. Oparin, J. Meyer-ter-Vehn, and S. I. Anisimov, Phys. Rev. Lett. **81**, 224 (1998).
30) D. von der Linde and K. Sokolowski-Tinten, Appl. Surf. Sci. **154–155**, 1 (2000).
31) J. Bonse, G. Bachelier, J. Siegel, and J. Solis, Phys. Rev. B **74**, 134106 (2006).
32) M. Domke, S. Rapp, M. Schmidt, and H. P. Huber, Opt. Express **20**, 10330 (2012).
33) X. Jia, T. Q. Jia, N. N. Peng, D. H. Feng, S. A. Zhang, and Z. R. Sun, J. Appl. Phys. **115**, 143102 (2014).
34) M. B. Agranat, S. I. Ashitkov, V. E. Fortov, A. V. Kirillin, A. V. Kostanovskii, S. I. Anisimov, and P. S. Kondratenko, Appl. Phys. A **69**, 637 (1999).
35) C. Guo, Microoptics Conf. (MOC), 2017 [DOI: 10.23919/MOC.2017.8244511].
36) N. A. Inogamov, Y. V. Petrov, V. V. Zhakhovsky, V. A. Khokhlov, B. J. Demaske, S. I. Ashitkov, K. V. Khishchenko, K. P. Migdal, M. B. Agranat, S. I. Anisimov, V. E. Fortov, and I. I. Oleynik, AIP Conf. Proc. **1464**, 593 (2012).
37) A. Cavalleri, K. Sokolowski-Tinten, J. Bialkowski, M. Schreiner, and D. von der Linde, J. Appl. Phys. **85**, 3301 (1999).
38) R. Fang, A. Y. Vorobyev, and C. Guo, Light: Sci. Appl. **6**, e16256 (2017).
39) G. D. Tsibidis, M. Barberoglou, P. A. Loukakos, E. Stratakis, and C. Fotakis, Phys. Rev. B **86**, 115316 (2012).
40) J. Bonse, S. M. Wiggins, and J. Solis, Appl. Surf. Sci. **248**, 151 (2005).
41) A. Ben-Yakar, A. Harkin, J. Ashmore, M. Shen, E. Mazur, R. L. Byer, and H. Stone, Proc. SPIE **4977**, 335 (2003).
42) M. E. Povarnitsyn, T. E. Itina, M. Sentis, K. V. Khishchenko, and P. R. Levashov, Phys. Rev. B **75**, 235414 (2007).
43) N. M. Bulgakova, R. Stoian, A. Rosenfeld, and I. V. Hetrtel, in *Laser-Surface Interactions for New Materials Production*, ed. A. Miotello and P. M. Ossi (Springer, Berlin/Heidelberg, 2010) Springer Series in Materials Science, Vol. 130, Chap. 4.
44) E. G. Gamaly and A. V. Rode, Prog. Quantum Electron. **37**, 215 (2013).
45) S. I. Anisimov and B. S. Luk'yanchuk, Phys. Usp. **45**, 293 (2002).
46) L. V. Zhigilei, Appl. Phys. A **76**, 339 (2003).
47) D. Perez and L. J. Lewis, Phys. Rev. Lett. **89**, 255504 (2002).
48) E. Leveugle, D. S. Ivanov, and L. V. Zhigilei, Appl. Phys. A **79**, 1643 (2004).
49) N. A. Inogamov, V. V. Zhakhovskii, S. I. Ashitkov, Y. V. Petrov, M. B. Agranat, S. I. Anisimov, K. Nishihara, and V. E. Fortov, J. Exp. Theor. Phys. **107**, 1 (2008).
50) N. A. Inogamov, A. Y. Faenov, V. V. Zhakhovskii, I. Y. Skobelev, V. A. Khokhlov, Y. Kato, M. Tanaka, T. A. Pikuz, M. Kishimoto, M. Ishino, M. Nishikino, Y. Fukuda, S. V. Bulanov, T. Kawachi, Y. V. Petrov, S. I. Anisimov, and V. E. Fortov, Contrib. Plasma Phys. **51**, 361 (2011).
51) D. S. Ivanov and L. V. Zhigilei, Phys. Rev. B **68**, 064114 (2003).
52) N. M. Bulgakova and I. M. Bourakov, Appl. Surf. Sci. **197–198**, 41 (2002).
53) B. J. Garrison, T. E. Itina, and L. V. Zhigilei, Phys. Rev. E **68**, 041501 (2003).
54) A. Miotello and R. Kelly, Appl. Phys. Lett. **67**, 3535 (1995).
55) S. I. Anisimov and B. Rethfeld, Proc. SPIE **3093**, 192 (1997).
56) A. Y. Vorobyev and C. Guo, J. Appl. Phys. **110**, 043102 (2011).
57) M. V. Shugaev and N. M. Bulgakova, Appl. Phys. A **101**, 103 (2010).
58) N. A. Inogamov, V. V. Zhakhovsky, V. A. Khokhlov, S. I. Ashitkov, Y. N. Emirov, K. V. Khichshenko, A. Y. Faenov, T. A. Pikuz, M. Ishino, M. Kando, N. Hasegawa, M. Nishikino, P. S. Komarov, B. J. Demaske, M. B. Agranat, S. I. Anisimov, T. Kawachi, and I. I. Oleynik, J. Phys.: Conf. Ser. **510**, 012041 (2014).
59) C. Wu, M. S. Christensen, J. M. Savolainen, P. Balling, and L. V. Zhigilei, Phys. Rev. B **91**, 035413 (2015).
60) A. Y. Vorobyev and C. Guo, Appl. Phys. Lett. **86**, 011916 (2005).
61) A. Y. Vorobyev and C. Guo, Opt. Express **14**, 13113 (2006).
62) N. M. Bulgakova, V. P. Zhukov, A. Y. Vorobyev, and C. Guo, Appl. Phys. A **92**, 883 (2008).
63) A. Y. Vorobyev and C. Guo, Appl. Phys. Lett. **102**, 074107 (2013).
64) E. C. Landis, K. C. Phillips, E. Mazur, and C. M. Friend, J. Appl. Phys. **112**, 063108 (2012).
65) A. Y. Vorob'ev, I. A. Dorofeev, and M. N. Libenson, Sov. Tech. Phys. Lett. **18**, 172 (1992).